energies

MDPI

Article

Time-Decoupling Layered Optimization for Energy and Transportation Systems under Dynamic Hydrogen Pricing

Hui Guo [1], Dandan Gong [1], Lijun Zhang [2,*], Wenke Mo [3], Feng Ding [3] and Fei Wang [1]

[1] School of Mechatronics Engineering and Automation, Shanghai University, Shanghai 200444, China; huiguo@shu.edu.cn (H.G.); DanniGDD@shu.edu.cn (D.G.); f.wang@shu.edu.cn (F.W.)
[2] Instituto Superior Técnico, University of Lisbon, 999022 Lisbon, Portugal
[3] Shanghai Marine Equipment Research Institute, Shanghai 200031, China; moco110@163.com (W.M.); shudf222@163.com (F.D.)
* Correspondence: lijun.zhang@tecnico.ulisboa.pt

Abstract: The growing popularity of renewable energy and hydrogen-powered vehicles (HVs) will facilitate the coordinated optimization of energy and transportation systems for economic and environmental benefits. However, little research attention has been paid to dynamic hydrogen pricing and its impact on the optimal performance of energy and transportation systems. To reduce the dependency on centralized controllers and protect information privacy, a time-decoupling layered optimization strategy is put forward to realize the low-carbon and economic operation of energy and transportation systems under dynamic hydrogen pricing. First, a dynamic hydrogen pricing mechanism was formulated on the basis of the share of renewable power in the energy supply and introduced into the optimization of distributed energy stations (DESs), which will promote hydrogen production using renewable power and minimize the DES construction and operation cost. On the basis of the dynamic hydrogen price optimized by DESs and the traffic conditions on roads, the raised user-centric routing optimization method can select a minimum cost route for HVs to purchase fuels from a DES with low-cost and/or low-carbon hydrogen. Finally, the effectiveness of the proposed optimization strategy was verified by simulations.

Keywords: layered optimization; renewable energy; hydrogen-powered vehicle; dynamic hydrogen pricing; routing optimization

Citation: Guo, H.; Gong, D.; Zhang, L.; Mo, W.; Ding, F.; Wang, F. Time-Decoupling Layered Optimization for Energy and Transportation Systems under Dynamic Hydrogen Pricing. *Energies* **2022**, *15*, 5382. https://doi.org/10.3390/en15155382

Academic Editor: Andrea Mariscotti

Received: 16 June 2022
Accepted: 21 July 2022
Published: 25 July 2022

1. Introduction

The energy and environmental crisis will promote the development of green transportation [1–3]. As low-carbon energy, green hydrogen can be used for decarbonization in long-distance transportation, especially in heavy trucks [4,5]. Therefore, the production of green hydrogen by water electrolysis using renewable energy, including photovoltaics and wind power, has been intensively studied [6,7].

Generally, green hydrogen production is relevant to the system planning and operation of energy stations based on renewable energy. Through reasonable capacity configuration and economical operation, energy stations can minimize construction and operating costs [8–10]. Among these, the reasonable formulation of hydrogen prices could increase the profit of energy stations and promote the production of hydrogen by electrolysis using renewable power, but they are scarcely investigated at present. In addition, pricing signals can be used to guide HVs to a DES with low-cost and/or low-carbon hydrogen aiming to satisfy the predefined quality of services, such as cost minimization and emission reduction [11–14].

At present, the routing optimization of electric vehicles can provide a reference for HVs [15,16]. Considering energy efficiency and charging price, an optimization model for EV fleet routing and charging was proposed in [17] to build a high-efficiency dynamic

transit system. Concerning battery electric range, a two-stage method to compute time-optimal routes for electric vehicles was proposed in [18], in which an adapted Moore–Bellman–Ford algorithm was used to solve the multi-objective shortest path problem. The charging price and trip time between different stations were considered in [19], and the joint problem of minimizing the average trip time and charging cost was formulated as a dual-objective convex optimization problem to realize routing optimization. The above study on routing optimization of electric vehicles (similar to HVs) can be divided into two categories: the user-centric routing optimization for a single vehicle and the system-centric routing optimization for multiple vehicles [20,21]. From the perspective of system-centric optimization, there are two issues. One is the dependence on a centralized controller and the information privacy of different users. On the other hand, a challenging problem is how to make multiple users follow the guidance of centralized controllers. This is more challenging because it involves the uncertain selfish behavior of users.

Considering the interaction between transportation and power networks, Zhang et al. [22] determined the site, size, and hourly operation of hydrogen refueling stations on the basis of simplified traffic flow models on a highway network. To reduce emissions in power and transportation systems, a coordinated planning strategy was presented in [23] to achieve the location planning of hydrogen refueling stations and optimize the penetration ratio of internal combustion vehicles, electric vehicles, and fuel cell vehicles. In [24], the aggregation of fast charging stations and electric vehicles was modeled as a leader–follower game and formulated as a bi-level optimization problem to increase benefits and provide regulation reserves for power systems. To reduce operation costs, a bilevel iteration optimization method was proposed in [25] to solve the coordinated optimization of hydrogen energy schedule and EV charging location selection. However, the existing joint optimization between power and transportation systems has not involved the dynamic hydrogen pricing mechanism used for DES optimization and the routing optimization of HVs [26–28].

To reduce the dependence on a centralized controller and protect information privacy, a time-decoupling layered optimization strategy under dynamic hydrogen pricing is presented to coordinate the optimization of DESs and HVs [29,30]. The main contributions are summarized as follows:

(1) Layered optimization of energy and transportation systems: confronted with the increasing penetration of renewable energy and HVs, a time-decoupling layered optimization strategy is proposed to realize the low-carbon economic operation of energy and transportation systems.
(2) DES planning and operation optimization based on dynamic hydrogen pricing. A novel dynamic hydrogen pricing mechanism is proposed and incorporated into the optimization of DES planning and operation, which will promote hydrogen production using renewable power and minimize the DES operation cost.
(3) User-centric routing optimization of HVs. On the basis of the dynamic hydrogen price optimized by the DES and the traffic condition on roads, the proposed user-centric routing optimization method can select a minimum cost route (MCR) for HVs to purchase fuels from a DES with low-cost and/or low-carbon hydrogen.

The rest is organized as follows. Section 2 introduces the proposed optimization strategy of energy and transportation systems. In Sections 3 and 4, the optimization of DES planning and operation based on dynamic hydrogen pricing and the user-centric routing optimization of HVs are described, respectively. Following that, the simulation results presented in Section 5 demonstrate the effectiveness of the proposed optimization strategy. Finally, Section 6 concludes this paper.

2. Time-Decoupling Layered Optimization Strategy

According to the different time scales of optimization objectives, the original optimization problem of energy and transportation systems can be decoupled into the two sub-problems shown in Figure 1, which are the optimization of DES planning and operation with a long time scale (year/day-level) and the user-centric routing optimization of HVs in real-time. In order to unify the time scale of DES planning and operation, the annual construction cost can be converted into the daily construction cost by the capital recovery factor. In addition to being influenced by the hourly changing hydrogen trading information, the user-centric routing optimization is also affected by the real-time traffic information (at the second level or minute level).

The uncertainty of renewable energy and load demands (including HVs) influences the safe and reliable operation of the system, which should be taken into account in the optimization strategy. To avoid the conservative solution obtained by robust optimization and the dependence on probability distributions of other methods, such as chance-constrained programming, uncertainties are processed through a data-driven stochastic model based on the scenarios in this paper, which can be built according to the clustering of historical data by the *k*-means algorithm [23,31].

Following that, the optimization of DES planning and operation under dynamic hydrogen pricing aims to minimize the total cost and promote hydrogen production using renewable power. On the basis of the dynamic hydrogen price optimized by DES and the traffic condition on roads, the HV as a user can select the MCR to purchase fuels from a DES with low-cost and/or low-carbon hydrogen.

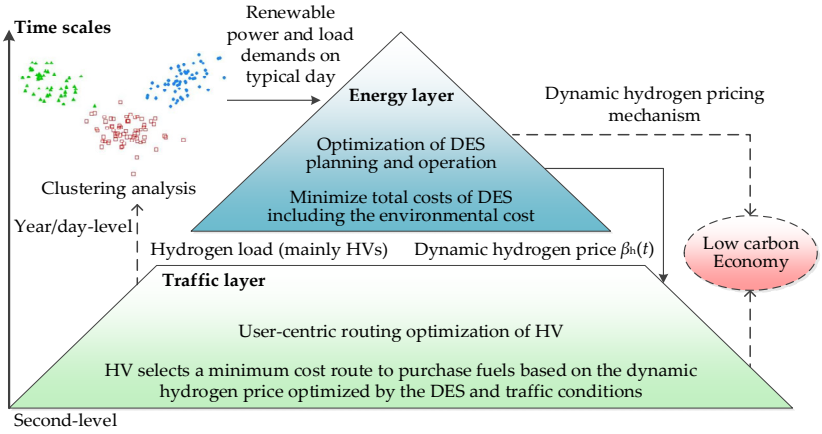

Figure 1. Proposed time-decoupling layered optimization strategy.

3. Energy Layer: Optimization of DES Planning and Operation

3.1. System Structure of DES

In addition to meeting a small quantity of electric/thermal/cooling load demands, the DES proposed in this paper mainly provides fuels for HVs, which can be viewed as a regionally integrated energy system, as shown in Figure 2. In this condition, the network constraints related to long-distance transmission can be ignored according to the model of a single energy hub [32,33].

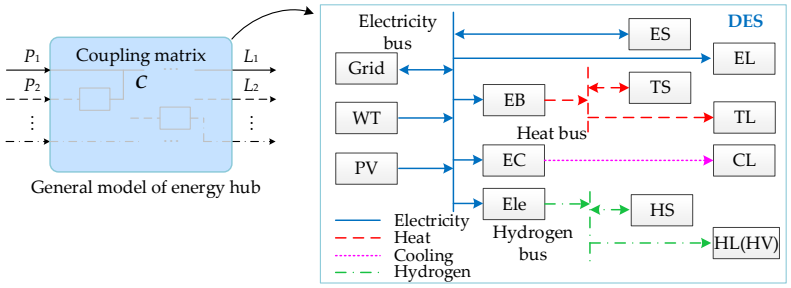

Figure 2. Example of DES system structure.

3.2. Optimization Model

1. Objective Function

The objective function of the optimization of DES planning and operation in the energy layer was formulated to minimize the total cost f, including construction cost f_{con}, operation and maintenance cost f_{ope}, environmental cost f_{env}, and transaction cost f_{tra}, as shown in (1):

$$\min f = f_{\text{con}} + f_{\text{ope}} + f_{\text{env}} + f_{\text{tra}} \tag{1}$$

- The construction cost f_{con} is represented by (2)–(4):

$$\begin{aligned} f_{\text{con}} &= R_k \sum_{k \in \Omega^k} \beta_k^{\text{con}} C_k, k \in \Omega^k \\ \Omega^k &= \{\text{EB}, \text{EC}, \text{Ele}, \text{ES}, \text{TS}, \text{HS}\} \end{aligned} \tag{2}$$

$$C_k = \sum_{k \in \Omega^k} \sum_{i=1}^{N_k} I_k^i C_k^i \tag{3}$$

$$R_k = \frac{r(1+r)^{y_k}}{(1+r)^{y_k} - 1} \tag{4}$$

where Ω^k is the set of candidate device k; β_k^{con} is the unit construction cost of candidate device k, (RMB/kWh); C_k is the installation capacity of candidate device k; R_k is the capital recovery factor of candidate device k; C_k^i is installation capacity class i of candidate device k; I_k^i is the 0/1 state variable of installation capacity class i for candidate device k, in which 0 indicates that the class i capacity of candidate device k is not selected, and 1 indicates that the class i capacity is selected; N_k is the total number of the installation capacity class for candidate device k; r is the annual interest rate; and y_k is the service life of candidate device k.

- The operation and maintenance cost f_{ope} is shown in (5):

$$f_{\text{ope}} = \sum_{t=1} \sum_{k \in \Omega^k} \beta_k^{\text{ope}} P_k(t) \tag{5}$$

where t is the index of scheduling time; β_k^{ope} is the unit operation cost of candidate device k, (RMB/kW); and $P_k(t)$ is the output power of candidate device k at time t.

- The environmental cost f_{env} can be calculated by (6):

To reduce the influence on the environment, the carbon emission cost of purchasing electricity from the utility grid should be considered.

$$f_{\text{env}} = \sum_{t=1} \gamma \alpha P_{\text{eb}}(t) \tag{6}$$

where γ is the carbon tax, (RMB/10^3 kg); α is the carbon emission intensity of purchasing electricity, (kg/kWh); and $P_{\text{eb}}(t)$ is the purchased electricity from the utility grid at time t.

- The transaction cost f_{tra} is described in (7):

The transaction cost includes the electricity purchase cost f_{eb}, the electricity sale revenue f_{es}, and the hydrogen sale profit f_{h}.

$$\begin{aligned} f_{\mathrm{tra}} &= f_{\mathrm{eb}} - f_{\mathrm{es}} - f_{\mathrm{h}} \\ &= \sum_{t=1} [\beta_{\mathrm{b}}(t) P_{\mathrm{eb}}(t) - \beta_{\mathrm{s}}(t) P_{\mathrm{es}}(t) - \beta_{\mathrm{h}}(t) P_{\mathrm{HL}}(t)] \end{aligned} \tag{7}$$

where $\beta_{\mathrm{b}}(t)$, $\beta_{\mathrm{s}}(t)$, and $\beta_{\mathrm{h}}(t)$ are the electricity purchase price, electricity sale price, and hydrogen sale price, respectively; $P_{\mathrm{es}}(t)$ is sale electricity power at time t; and $P_{\mathrm{HL}}(t)$ is sale hydrogen power, which is equal to the hydrogen demand of HVs in the traffic layer.

It should be noted that the dynamic hydrogen pricing mechanism was designed to correlate with the proportion of renewable power in the energy supply, as shown in (8)–(10). In addition, the hydrogen price is limited by the hydrogen price margin in the market, which cannot increase arbitrarily to pursue higher profits, as shown in (28) [8].

$$\beta_{\mathrm{h}}(t) = \beta_{\mathrm{h}}^{\min} + \beta_{\mathrm{h,adj}}(t) \tag{8}$$

$$\beta_{\mathrm{h,adj}}(t) = a_{\mathrm{h}} \left(\frac{P_{\mathrm{Ele,in}}(t)}{P_{\mathrm{Re}}(t)}\right)^2 + b_{\mathrm{h}} \left(\frac{P_{\mathrm{Ele,in}}(t)}{P_{\mathrm{Re}}(t)}\right) + c_{\mathrm{h}} \tag{9}$$

$$P_{\mathrm{Re}}(t) = P_{\mathrm{WT}}(t) + P_{\mathrm{PV}}(t) \tag{10}$$

where $\beta_{\mathrm{h}}^{\min}$ is the minimum hydrogen sale price, (RMB/kWh); $\beta_{\mathrm{h,adj}}(t)$ is the slack variable of the hydrogen sale price at time t, (RMB/kWh); a_{h}, b_{h}, and c_{h} are the coefficients of the slack variable function for the hydrogen sale price; $P_{\mathrm{Ele,in}}(t)$ is the input power of Els at time t; $P_{\mathrm{Re}}(t)$ is the total power of renewable energy at time t; $P_{\mathrm{PV}}(t)/P_{\mathrm{WT}}(t)$ is the generation power of PV/WT at time t. The slack variable shown in (9) is set to be varied with the proportion of renewable energy in the energy supply in order to promote hydrogen production using renewable energy.

2. Equipment Constraints

- Electric boiler (EB):

$$P_{\mathrm{EB}}(t) = \eta_{\mathrm{EB}} P_{\mathrm{EB,in}}(t) \tag{11}$$

$$\mu_{\mathrm{EB}}^{\min} C_{\mathrm{EB}} \le P_{\mathrm{EB}}(t) \le \mu_{\mathrm{EB}}^{\max} C_{\mathrm{EB}} \tag{12}$$

where $P_{\mathrm{EB,in}}(t)$ is the input power of EB at time t; η_{EB} is the conversion efficiency of EB; and $\mu_{\mathrm{EB}}^{\min}$ and $\mu_{\mathrm{EB}}^{\max}$ are the minimum and maximum power factors of EB, respectively.

- Electric cooling (EC):

$$P_{\mathrm{EC}}(t) = \lambda_{\mathrm{EC}} P_{\mathrm{EC,in}}(t) \tag{13}$$

$$\mu_{\mathrm{EC}}^{\min} C_{\mathrm{EC}} \le P_{\mathrm{EC}}(t) \le \mu_{\mathrm{EC}}^{\max} C_{\mathrm{EC}} \tag{14}$$

where $P_{\mathrm{EC,in}}(t)$ is the input power of EC at time t; λ_{EC} is the performance coefficient of EC; $\mu_{\mathrm{EC}}^{\min}$ and $\mu_{\mathrm{EC}}^{\max}$ are the minimum and maximum power factors of EC, respectively.

- Electrolysis (Ele):

$$P_{\mathrm{Ele}}(t) = \lambda_{\mathrm{Ele}}(t) P_{\mathrm{Ele,in}}(t) \tag{15}$$

$$\lambda_{\mathrm{Ele}}(t) = a_{\mathrm{Ele}} \left(\frac{P_{\mathrm{Ele,in}}(t)}{P_{\mathrm{Ele}}^{\mathrm{rat}}}\right)^2 + b_{\mathrm{Ele}} \left(\frac{P_{\mathrm{Ele,in}}(t)}{P_{\mathrm{Ele}}^{\mathrm{rat}}}\right) + c_{\mathrm{Ele}} \tag{16}$$

$$\mu_{\mathrm{Ele}}^{\min} C_{\mathrm{Ele}} \le P_{\mathrm{Ele}}(t) \le \mu_{\mathrm{Ele}}^{\max} C_{\mathrm{Ele}} \tag{17}$$

where $P_{\mathrm{Ele,in}}(t)$ is the input power of Ele at time t; $\lambda_{\mathrm{Ele}}(t)$ is the conversion efficiency of Ele at time t; a_{Ele}, b_{Ele}, and c_{Ele} are the coefficients of the conversion efficiency function for Ele; $P_{\mathrm{Ele}}^{\mathrm{rat}}$ is the rated power of Ele; and $\mu_{\mathrm{Ele}}^{\min}$ and $\mu_{\mathrm{Ele}}^{\max}$ are the minimum and maximum power factors of Ele, respectively.

- Storage equipment (including electrical (EES)/thermal (TES)/hydrogen (HES) energy storage corresponding to d = 4, 5, and 6):

$$\begin{gathered} \mu_{k,\mathrm{cap}}^{\min} C_k \le C_k(t) \le \mu_{k,\mathrm{cap}}^{\max} C_k,\ k \in \Omega^k \\ \Omega^k = \{\mathrm{EB}, \mathrm{EC}, \mathrm{Ele}, \mathrm{ES}, \mathrm{TS}, \mathrm{HS}\} \end{gathered} \tag{18}$$

$$C_k(t) = (1-\zeta_k)C_k(t-1) + \eta_{k,\mathrm{c}} P_{k,\mathrm{c}}(t) - P_{k,d}(t)/\eta_{k,d} \tag{19}$$

$$\mu_{k,\mathrm{c}}^{\min} C_k \le P_{k,\mathrm{c}}(t) \le \mu_{k,\mathrm{c}}^{\max} C_k \tag{20}$$

$$\mu_{k,d}^{\min} C_k \le P_{k,d}(t) \le \mu_{k,d}^{\max} C_k \tag{21}$$

$$P_{k,d}(t) P_{k,\mathrm{c}}(t) = 0 \tag{22}$$

$$C_k(1) = C_k(\mathrm{T}) \tag{23}$$

where $C_k(t)$ is the capacity of storage device k at time t; $\mu_{k,\mathrm{cap}}^{\min}$ and $\mu_{k,\mathrm{cap}}^{\max}$ are the minimum and maximum capacity factors of storage device k, respectively; ζ_k is the self-loss coefficient of storage device k; $\eta_{k,\mathrm{c}}$ and $\eta_{k,d}$ are the charging and discharging efficiencies of storage device k, respectively; $P_{k,\mathrm{c}}(t)$ and $P_{k,d}(t)$ are the charging and discharging powers of storage device k at time t, respectively; $\mu_{k,\mathrm{c}}^{\min}$ and $\mu_{k,\mathrm{c}}^{\max}$ are the minimum and maximum charging power factors of storage device k, respectively; and $\mu_{k,d}^{\min}$ and $\mu_{k,d}^{\max}$ are the minimum and maximum discharging power factors of storage device k, respectively.

3. System Constraints of DES

- Equipment selection:

In order to select the installation capacity class i for candidate device k, the constraint shown in (24) should be satisfied.

$$\begin{gathered} \sum_{i=1}^{N_i} I_k^i = 1,\ k \in \Omega^k \\ \Omega^k = \{\mathrm{EB}, \mathrm{EC}, \mathrm{Ele}, \mathrm{ES}, \mathrm{TS}, \mathrm{HS}\} \end{gathered} \tag{24}$$

Note that renewable energy generation equipment of WT and PV is regarded as indispensable equipment for DESs.

- Transaction power with the utility grid:

$$0 \le P_{\mathrm{eb}}(t) \le P_{\mathrm{eb}}^{\max} \tag{25}$$

$$0 \le P_{\mathrm{es}}(t) \le P_{\mathrm{es}}^{\max} \tag{26}$$

$$P_{\mathrm{eb}}(t) P_{\mathrm{es}}(t) = 0 \tag{27}$$

where $P_{\mathrm{eb}}^{\max}$ and $P_{\mathrm{es}}^{\max}$ are the maximum purchase and sale of electricity, respectively.

- Hydrogen sale price:

$$0 \leq \beta_{\mathrm{h}}(t) \leq \beta_{\mathrm{h}}^{\max} \tag{28}$$

- Power balance (including electricity, heat, cooling, and hydrogen balance):

$$\begin{aligned} &P_{\mathrm{eb}}(t) - P_{\mathrm{es}}(t) + P_{\mathrm{WT}}(t) + P_{\mathrm{PV}}(t) + P_{\mathrm{ES},d}(t) \\ &= P_{\mathrm{EB,in}}(t) + P_{\mathrm{EC,in}}(t) + P_{\mathrm{Ele,in}}(t) + P_{\mathrm{EL}}(t) + P_{\mathrm{ES,c}}(t) \end{aligned} \tag{29}$$

$$P_{\mathrm{EB}}(t) + P_{\mathrm{TS},d}(t) = P_{\mathrm{TL}}(t) + P_{\mathrm{TS,c}}(t) \tag{30}$$

$$P_{\mathrm{EC}}(t) = P_{\mathrm{CL}}(t) \tag{31}$$

$$P_{\mathrm{Ele}}(t) + P_{\mathrm{HS},d}(t) = P_{\mathrm{HL}}(t) + P_{\mathrm{HS,c}}(t) \tag{32}$$

where $P_{\mathrm{EL}}(t)$, $P_{\mathrm{TL}}(t)$, and $P_{\mathrm{CL}}(t)$ are the electrical load, thermal load, and cooling load at time t, respectively.

4. Traffic Layer: User-Centric Path Optimization of HVs

After the optimization of DES planning and operation, according to the shared information of hydrogen transactions and traffic conditions on roads, the HV, as a user, can select the MCR to purchase fuels by the raised user-centric routing optimization method based on graph theory.

4.1. Graph Model of Traffic Roads

Since renewable energy and HVs are decentralized, the DESs, which are the same as hydrogen fuel stations, are usually located at road junctions, and there are road connections between multiple DESs, as shown in Figure 3. The model of traffic roads is described as the graph $G = \{V, E\}$ with weight and direction. Specifically, the road junction constitutes the node set $V = \{1, 2, \cdots, a, b, \cdots\}$, and the road segment constitutes the edge set $E = \{(1,2), \cdots, (a,b), \cdots\}$. Furthermore, the edge weight $f_{(a,b)}$ indicates the transportation cost of HVs on road (a,b), and the edge direction indicates the traffic direction of roads. As a note, some road junctions may be the origin/destination of HVs and the location of DESs. If the road junction is the location of DES d, the node weights β_d and F_d represent the hydrogen sale price and volume of DES d. Once the transaction information of the DES changes, it is broadcasted to the HVs.

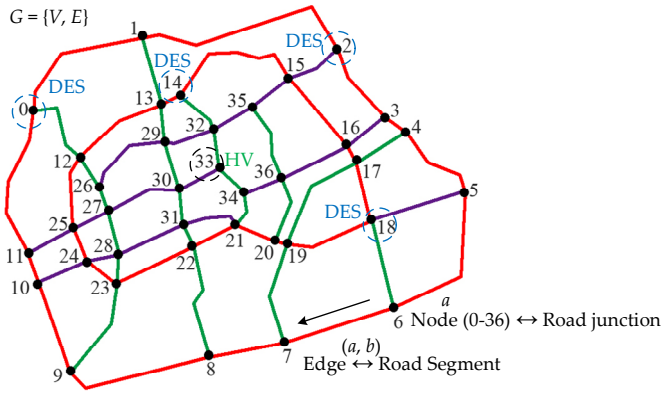

Figure 3. Graph model of traffic roads.

4.2. Routing Optimization

In graph model G of traffic roads, the total number of nodes is expressed as N_G. At time t after DES optimization, the DES becomes a seller d ($d \in N_G$) of hydrogen to HVs. They send their transaction information (hydrogen sale price $\beta_d = \beta_h(t)$ and hydrogen sale volume $F_d = P_{HL}(t)\Delta t$) to the HVs, and then the HV, as a user, makes a response to the selected DES according to the results of routing optimization.

1. Selection of MCR

The objective of user-centric routing optimization is the selection of the MCR for HV on the basis of the shared information of hydrogen transaction and traffic conditions, which is expressed to minimize the hydrogen refueling cost $f_{R:i\to d}$ of HVs to purchase fuels from origin i to destination d, including the transportation cost $\sum_{(a,b)\in R} w_{(a,b)} f_{(a,b)}$ incurred during the route $R : i \to d$ and the transaction cost $\sum_{d\in R} w_d f_{i-d}$ between HV i and DES d, as shown in (33):

$$\min f_{R:i\to d} = \sum_{(a,b)\in R} w_{(a,b)} f_{(a,b)} + \sum_{d\in R} w_d f_{i-d} \tag{33}$$

$$f_{(a,b)} = \beta_0 (L_{(a,b)} / v_{(a,b)}) \tag{34}$$

$$v_{(a,b)} = v^{\text{fre}}_{(a,b)} (1 - \rho_{(a,b)} / \rho^{\text{jam}}_{(a,b)}) \tag{35}$$

$$f_{i-d} = \beta_d F_i \tag{36}$$

where $w_{(a,b)}$ and w_d are non-negative weight coefficients, which influence the optimal selection of road (a, b) and DES d. A large $w_{(a,b)}$ indicates that road (a, b) is more prone to traffic congestion and vice versa. A large w_d indicates that DES d is more prone to refueling congestion and vice versa. β_0 is the transportation cost per unit time; $L_{(a,b)}$ is the distance of road (a, b); $v_{(a,b)}$ is the velocity of HV i on road (a, b); $v^{\text{fre}}_{(a,b)}$ is the zero flow velocity on road (a, b), $\rho_{(a,b)}$ is the traffic density on road (a, b), $\rho^{\text{jam}}_{(a,b)}$ is the jamming density on road (a, b), approximately 143 veh/h [26]; and F_i indicates the hydrogen purchase volume of HV i.

2. Transaction Constraints

Equations (37) and (38) indicate that the hydrogen purchase volume of HV F_i should not exceed the hydrogen sale volume of DES F_d, and the remaining hydrogen of DES needs to be updated.

$$F_i \le F_d \tag{37}$$

$$F_d = F_d - F_i \tag{38}$$

3. Traffic Constraints

For HV i, the selected DES d should satisfy the requirement of minimum remaining mileage $SL^{\min}_i$, and the remaining mileage SL_i of HV i needs to be updated according to the distance of route $L_{R:i\to d}$.

$$SL^{\min}_i \le SL_i \tag{39}$$

$$SL_i = SL_i - L_{R:i\to d} \tag{40}$$

The traffic density on road (a, b) should not exceed the jamming density, which represents the road capacity.

$$\rho_{(a,b)} \le \rho^{\text{jam}}_{(a,b)} \tag{41}$$

The velocity of HVs on road (a, b) should not exceed the zero-flow velocity.

$$v_{(a,b)} \le v^{\text{fre}}_{(a,b)} \tag{42}$$

The time spent on the MCR for HV i is limited by the update time of the dynamic hydrogen price:

$$\sum_{(a,b)\in R} L_{(a,b)}/v_{(a,b)} \leq RT_i \tag{43}$$

where RT_i represents the remaining time from HV i current routing optimization to the next hour.

5. Simulation Results and Analysis

Corresponding to the time-decoupling layered optimization strategy shown in Figure 1, the decoupled optimization problems of the energy and transportation system under dynamic hydrogen pricing were solved in two stages on a computer with an Intel Core i7 3.60 GHz CPU and 16 GB of RAM. As a subproblem, the routing optimization of the HVs was solved by the proposed user-centric routing optimization method based on shortest path algorithms, as shown in Figure 4.

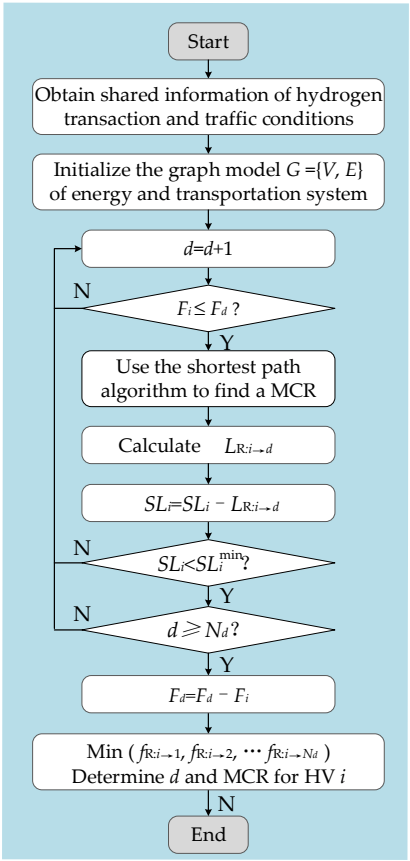

Figure 4. Flowchart of the user-centric routing optimization method. N_d represents the total number of candidate DESs.

5.1. Energy Layer: Optimization of DES Planning and Operation

As a representative of the DES shown in Figure 2, DES 0, with the following parameters, was designed and taken as a simulation case to analyze.

1. Basic Data

According to the historical data at the annual level, the district is classified into s heating season (120 cumulative days), s cooling season (100 cumulative days), and s transition season (145 cumulative days) considering the seasonal variation and typical diurnal variation. Figure 5 provides the renewable energy power and load demands on a typical day in the above three seasons for DES 0 in the district [34]. In addition, the

time-of-use electricity price is shown in Figure 6 [35], and the basic parameters of candidate conversion/storage equipment are shown in Tables 1 and 2 [36].

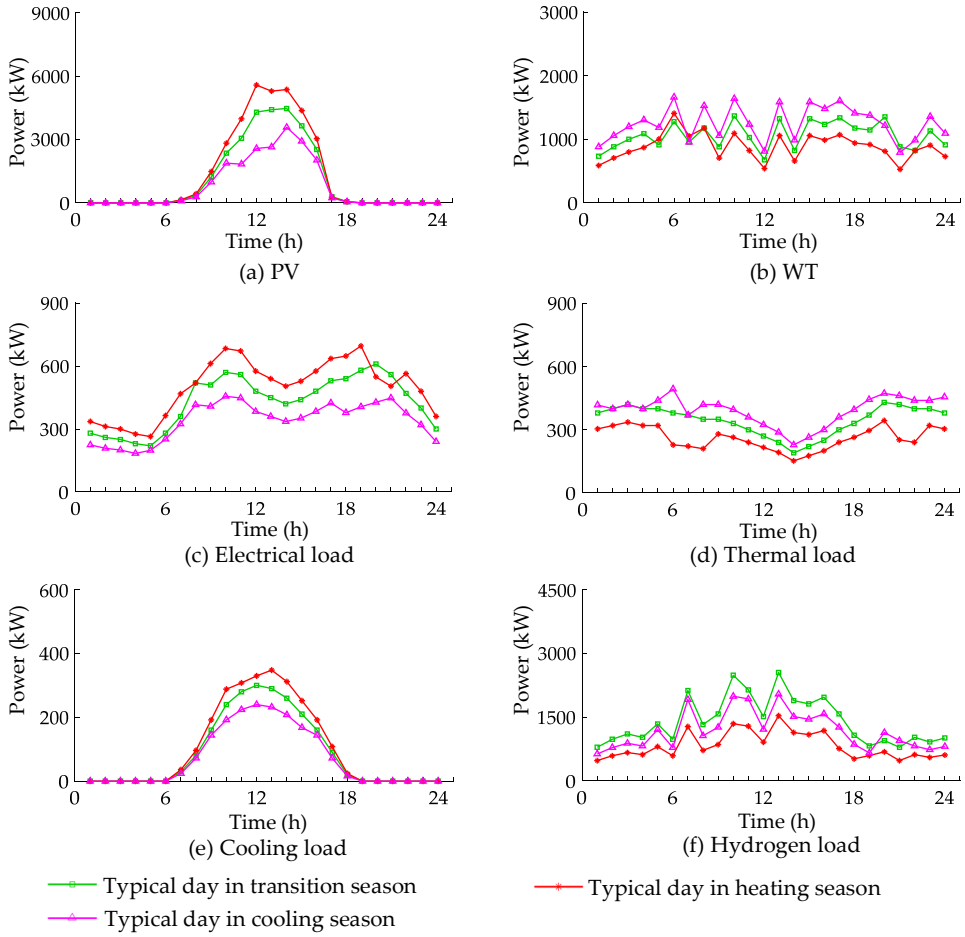

Figure 5. Renewable energy generation and load demands in a typical day for DES 0.

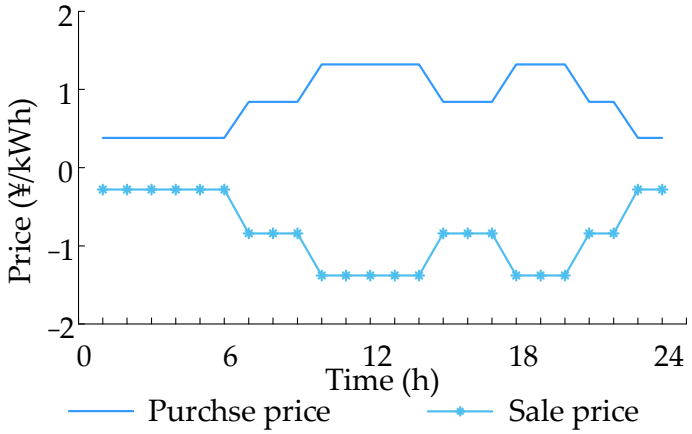

Figure 6. Time-of-use electricity price.

Table 1. Parameters of candidate conversion equipment in DES 0.

Conversion Equipment	Class	Capacity (kW)	Unit Construction Cost (RMB/kW)	Unit Operation Cost (RMB/kW)	Conversion Coefficient	Life (Year)
Electric cooling	EC1	100	800	0.008	3	20
	EC2	500	800	0.008	3	20
Electrolysis	Ele1	1000	12,000	0.16	/	10
	Ele2	2000	12,000	0.16	/	10
	Ele3	3000	12,000	0.16	/	10
Electric boiler	EB1	500	1000	0.02	3	10
	EB2	1000	1000	0.02	3	10
	EB3	1500	1000	0.02	3	10

Table 2. Parameters of candidate storage equipment in DES 0.

Storage Equipment	Class	Capacity (kW)	Unit Construction Cost (RMB/kW)	Unit Operation Cost (RMB/kW)	Self-Loss Coefficient	Charging/Discharging Efficiency
Electricity	ES1	1000	1700	0.0018	0.001	0.95
	ES2	2000	1700	0.0018	0.001	0.95
Heat	TS1	300	190	0.0016	0.01	0.85
	TS2	1000	190	0.0016	0.01	0.85
Hydrogen	HS1	500	1800	0.01	0.01	0.85
	HS2	1000	1800	0.01	0.01	0.85

2. Optimal Results

System Planning: In general, a too-large capacity configuration causes resource waste, while a small-capacity configuration reduces the system's safety and reliability. According to the data on renewable energy generation and load demands on a typical day in each of the three seasons, the equipment selection and capacity configuration were solved reasonably, as shown in Figure 7. Consequently, the goal of minimizing system construction and operation cost was achieved successfully, which will increase the system's operation flexibility and economy.

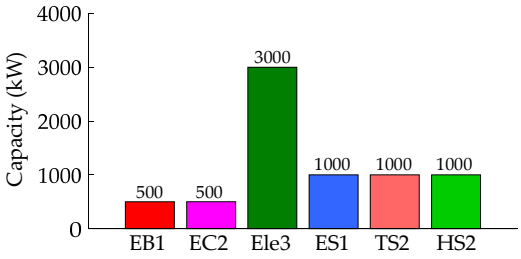

Figure 7. Equipment selection and capacity configuration of DES 0.

- Operation Optimization in DES 0:

As an example, the optimal operation on a typical day in the transition season was selected to analyze in detail. Figure 8 shows the optimization results of energy conversion and storage equipment. It can be inferred from the figures that the power balance of electricity, heat, cooling, and hydrogen in the DES was achieved. From the quantitative perspective, because DES 0 mainly provides fuels for HVs, the load demands of electricity, heat, and cooling were relatively small.

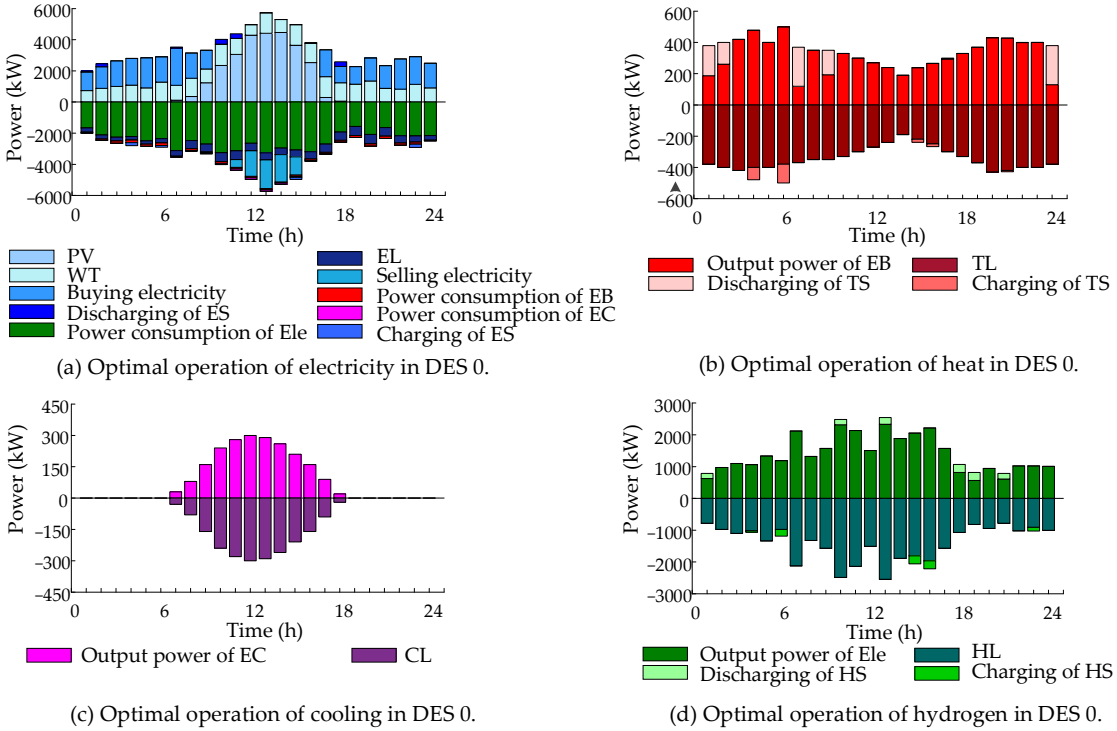

(a) Optimal operation of electricity in DES 0.

(b) Optimal operation of heat in DES 0.

(c) Optimal operation of cooling in DES 0.

(d) Optimal operation of hydrogen in DES 0.

Figure 8. Optimal operation in DES 0.

- Dynamic Hydrogen Pricing:

As shown in Figure 9 and Table 3, the dynamic hydrogen pricing of DES 0 was achieved and mainly varied with the proportion of renewable power.

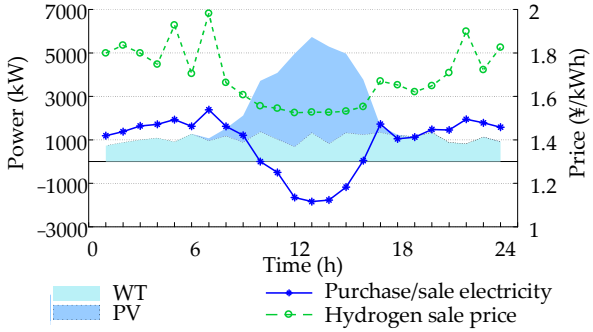

Figure 9. Optimal results of dynamic hydrogen pricing for DES 0.

Table 3. Hydrogen transaction information for DES 0.

Time	Sale Price (RMB/kWh)	Sale Volume (kWh)	Time	Sale Price (RMB/kWh)	Sale Volume (kWh)
1:00	1.7992	786	13:00	1.5276	2546.6
2:00	1.8354	974.6	14:00	1.5267	1886.4
3:00	1.7992	1100.4	15:00	1.5316	1807.8
4:00	1.7479	1021.8	16:00	1.5528	1965
5:00	1.9277	1336.2	17:00	1.6701	1572
6:00	1.7084	974.6	18:00	1.6529	1069
7:00	1.9820	2122.2	19:00	1.6210	817.4
8:00	1.6634	1320.5	20:00	1.6488	943.2
9:00	1.6069	1572	21:00	1.7087	786
10:00	1.5559	2483.8	22:00	1.8995	1021.8
11:00	1.5448	2137.9	23:00	1.7225	911.8
12:00	1.5248	1509.1	24:00	1.8256	1006.1

From 1:00 to 6:00 and 18:00 to 24:00 (Figure 9), the PV power was basically zero, and the total power of renewable energy was small. In order to satisfy the hydrogen load demands, DES 0 purchased electricity from the utility grid with a relatively low electricity sale price to produce hydrogen by water electrolysis. Therefore, the hydrogen sale price during those time slots was relatively high. From 10:00 to 16:00, with an increase in the PV power, the total power of renewable energy became larger. Most of the electricity consumed by electrolysis for hydrogen production was supplied by renewable energy, so the hydrogen sale price during this period was relatively low. Furthermore, the surplus electricity generated by renewable energy was sold to the utility grid at a relatively high electricity sale price for a certain profit, as shown in Figure 6.

The simulation results proved that the dynamic hydrogen pricing was mainly related to the proportion of renewable power in the energy supply. When the proportion of renewable power in the energy supply increased, the hydrogen sale price decreased. Conversely, when the proportion of renewable power in the energy supply decreased, the hydrogen sale price increased, as shown in Figure 9.

- Comparison with Fixed Hydrogen Price:

According to the cost details of the two scenarios shown in Table 4, a better optimization performance of the proposed strategy on DES total cost and carbon emissions was obtained. Specifically, the total cost in scenario 2 was negative, and the absolute value was larger, which means it had more system benefits. The environmental cost in scenario 2 was lower, which means it had fewer carbon emissions.

Table 4. Cost details of different scenarios.

Cost (RMB) \ Case	Scenario 1	Scenario 2
Construction cost f_{con}	15,642	15,642
Operation and maintenance cost f_{ope}	5925	5912
Environmental cost f_{env}	501	496
Electricity purchase cost f_{eb}	18,708	18,158
Electricity sale revenue f_{es}	−9192	−8448
Hydrogen sale profit f_{h}	−50,508	−56,166
Total	−18,925	−24,406

Scenario 1: fixed hydrogen price; scenario 2: proposed dynamic hydrogen price; negative costs represent benefits.

5.2. Traffic Layer: User-Centric Routing Optimization of HVs

1. Basic Data

On the basis of the optimal results of the energy layer, the hydrogen sale price and volume of DES 0 at 5:00 and 24:00 on a typical day in the transition season can be obtained from Table 3 and is listed in Table 5 (converted to the corresponding mass units). In addition, the transaction information on other DESs and HVs is provided in Table 5 in order to analyze the routing optimization of HVs. Furthermore, Table 6 provides the parameters of the traffic roads shown in Figure 3, which are simplified from the actual road [23].

2. Optimal Results

The optimal results of user-centric routing optimization for HVs are shown in Table 7, including the selected DES, the MCR, and hydrogen refueling costs. Specifically, the optimal route and the DES were selected by jointly considering the transportation cost (TPC) and transaction cost (TAC). The transportation cost is related to the traffic conditions (including the direction, distance, zero flow velocity, and maximum vehicle flow) on the roads. The transaction cost is mainly influenced by the hydrogen sale price and volume.

Table 5. Hydrogen transaction information of HVs and DESs.

Time		Price (RMB/kg)	Volume (kg)
5:00	HV 33	/	6.5
	DES 0	30.3034	85
	DES 2	29.9277	80
	DES 14	30.3034	85
	DES 18	30.3018	75
24:00	HV 26	/	5
	DES 0	28.6984	64
	DES 1	27.6075	63
	DES 11	25.8060	60

Table 6. Parameters of traffic roads (0–36 nodes).

Line	Distance (km)	Zero Flow Velocity (km/h)	Line	Distance (km)	Zero Flow Velocity (km/h)
(0,1)	7.9	70	(16,17)	1.0	50
(0,11)	7.7	70	(16,36)	3.9	50
(0,12)	4.1	70	(17,18)	3.1	50
(1,2)	12.3	70	(17,19)	7.6	50
(1,13)	3.3	70	(18,19)	4.9	50
(2,3)	4.3	70	(19,20)	0.8	50
(2,15)	2.3	70	(20,21)	1.9	50
(3,4)	1.1	70	(20,36)	3.6	50
(3,16)	2.5	70	(21,22)	2.2	50
(4,5)	4.9	70	(21,31)	3.3	40
(4,17)	2.8	70	(21,34)	1.7	40
(5,6)	8.6	70	(22,23)	4.7	50
(5,18)	4.8	70	(22,31)	1.4	40
(6,7)	5.9	70	(23,24)	2.0	50
(6,18)	4.7	70	(23,28)	1.5	50
(7,8)	4.1	70	(24,25)	2.1	50
(7,19)	5.8	70	(24,28)	2.0	50
(8,9)	7.7	70	(25,27)	2.5	50
(8,22)	5.8	70	(26,27)	1.4	50
(9,10)	5.4	70	(26,29)	3.8	50
(9,23)	4.9	70	(27,28)	2.8	50
(10,11)	1.6	70	(27,30)	3.9	50
(10,24)	2.8	70	(28,31)	3.9	50
(11,25)	2.8	70	(29,30)	2.5	40
(12,13)	4.5	50	(29,32)	2.8	40
(12,25)	4.4	50	(30,31)	2.1	40
(12,26)	1.9	50	(30,33)	3.0	40
(13,14)	1.5	50	(31,34)	1.5	40
(13,29)	1.7	50	(32,33)	2.2	40
(14,15)	7.8	50	(32,35)	2.1	40
(14,32)	2.4	50	(33,34)	1.7	40
(15,16)	4.3	50	(34,36)	2.4	40
(15,35)	1.5	50	(35,36)	4.0	50

- Influence of the Road Direction:

The vehicle flows of all roads shown in Figure 3 are zero at 5:00, assuming that all roads are two-way in scenario 1, whereas in scenario 2, all roads are two-way except for road (32,14).

As shown in Table 5, to satisfy the fuel demands of HV 33 at 5:00, the candidate energy stations were DES 0, 2, 14, and 18. During this period, the transaction costs of the candidate DESs were relatively close, so the selection of MCR mainly depended on the transportation cost.

According to the total cost including transportation cost and transaction cost shown in Table 7, the MCR of HV 33 was 33→32→14 in scenario 1, and the energy station selected to purchase fuels was DES 14. In scenario 2, because road (32,14) was impassable, the MCR of HV 33 changed to 33→32→35→15→2 instead of 33→32→14 in scenario 1. It can be concluded that the direction of roads not only affects the selection of MCR but may also influence the selection of candidate DESs.

Table 7. Optimal results of HV routing optimization.

Scenario		HV *i*	DES *d*	Minimum-Cost Route	TPC (RMB)	TAC (RMB)	Total Cost (RMB)
5:00	1	33	0	33→30→27→26→12→0	41.64	196.97	238.61
			2	33→32→35→15→2	25.55	194.53	220.08
			14	**33→32→14**	**15.45**	**196.97**	**212.42**
			18	33→34→21→20→19→18	35.55	196.96	232.51
	2	33	0	33→30→27→26→12→0	41.64	196.97	238.61
			2	**33→32→35→15→2**	**25.55**	**194.53**	**220.08**
			14	33→32→29→13→14	28.35	196.97	225.32
			18	33→34→21→20→19→18	35.55	196.96	232.51
24:00	1	26	0	26→12→0	14.49	143.49	157.98
			1	26→29→13→1	23.57	138.04	161.61
			11	**26→27→25→11**	**17.70**	**129.03**	**146.73**
	2	26	0	26→12→0	14.49	143.49	157.98
			1	26→29→13→1	23.57	138.04	161.61
			11	**26→27→25→24→10→11**	**27.43**	**129.03**	**156.46**
	3	26	**0**	**26→12→0**	**14.49**	**143.42**	**157.91**
			1	26→29→13→1	23.57	143.42	166.99
			11	26→27→25→11	17.70	143.42	161.12

- Influence of the Vehicle Flow on Roads:

If all roads shown in Figure 3 are two-way at 24:00, it is supposed that the vehicle flows of all roads are zero in scenario 1, whereas in scenario 2, the vehicle flows of all roads are zero except for road (25,11), which has 250 vehicles (meaning high traffic density).

As shown in Table 5, to satisfy the fuel demands of HV 26 at 24:00, the candidate energy stations were DES 0, 1, and 11. During this period, the hydrogen sale prices of candidate DESs were different, so the selection of the optimal path and DES depended on the total cost, including the transportation cost and transaction cost.

According to the total cost shown in Table 7, the MCR of HV 26 in scenario 1 was 26→27→25→11, and the energy station selected to purchase fuels was DES 11, which had a lower hydrogen sale price. In scenario 2, the vehicle flows on road (25,11) changed from zero to 250 vehicles, so the transportation cost on the road (25,11) increased accordingly, causing the MCR of HV 29 to change to 26→27→25→24→10→11. It can be seen from the results that the pre-existing vehicle flow (meaning traffic density) on roads may affect the selection of the MCR and even the candidate DES for HVs.

- Influence of the Dynamic Hydrogen Price (compared with the fixed hydrogen price):

If all roads shown in Figure 3 are two-way at 24:00, it is supposed that the vehicle flows of all roads are zero in scenarios 1 and 3, whereas in scenario 3, the hydrogen prices of DES 0, 1, and 11 are uniformly set to the fixed 28.6842 RMB/kg. The fixed hydrogen price in scenario 3 is set to the mean value of the given price range to avoid one-sidedness in comparison with scenario 1.

According to the joint consideration of transportation cost and transaction cost in scenario 1, HV 26, as a user, selects MCR: 26→27→25→11 to purchase fuels from DES 11 with a lower hydrogen sale price. In scenario 3, the selection of MCR: 26→12→0 for HV 26 is only determined by the transportation cost. Under this condition, the price signal cannot be used to guide the HV to purchase fuels from a DES with low-cost and/or low-carbon hydrogen.

On the basis of the joint consideration of transportation costs and transaction costs (related to the shared information of traffic conditions and hydrogen transactions), the HV, as a user, can select the MCR to purchase fuels. In addition, the traffic congestion on the road can be considered by increasing the weight coefficient of transportation costs, and the refueling congestion in DESs can be taken into account by adjusting the weight coefficient of the transaction costs.

6. Conclusions

The growing popularity of renewable energy and hydrogen-powered vehicles (HVs) will facilitate the coordinated optimization of energy and transportation systems for economic and environmental benefits. To reduce the dependence on centralized controllers and protect the information privacy of DESs and HVs, a time-decoupling layered optimization strategy under dynamic hydrogen pricing is proposed. By incorporating the presented dynamic hydrogen pricing mechanism into the optimization of DES planning and operation, the system cost minimization and emission reduction were achieved. On the basis of the dynamic hydrogen price optimized by DESs and traffic conditions on roads, the HV, as a user, successfully selected the MCR to purchase fuels from a DES with low-cost and/or low-carbon hydrogen by applying the proposed routing optimization method.

Author Contributions: Conceptualization, L.Z.; methodology, H.G.; software, D.G.; validation, H.G.; formal analysis, L.Z. and F.W.; investigation, D.G. and F.D.; resources, F.W. and W.M.; data curation, L.Z. and F.D.; writing—original draft preparation, H.G. and D.G.; writing—review and editing, H.G. and L.Z.; visualization, D.G.; supervision, F.W. and W.M. All authors have read and agreed to the published version of the manuscript.

Funding: This work was supported in part by the National Natural Science Foundation of China under Grant 52107199 and the International Corporation Project of the Shanghai Science and Technology Commission under grant 21190780300.

Institutional Review Board Statement: Not applicable.

Informed Consent Statement: Not applicable.

Conflicts of Interest: The authors declare no conflict of interest.

Abbreviations

DES	Distributed energy station
HV	Hydrogen-powered vehicle
EV	Electric vehicle
MCR	Minimum-cost route
WT	Wind turbine
PV	Photovoltaics

EB	Electric boiler
EC	Electric cooling
Ele	Electrolysis
ES	Electrical storage
TS	Thermal storage
HS	Hydrogen storage
EL	Electrical load
TL	Thermal load
CL/HL	Cooling/hydrogen load

References

1. Xia, F.; Rahim, A.; Kong, X.; Wang, M.; Cai, Y.; Wang, J. Modeling and Analysis of Large-Scale Urban Mobility for Green Transportation. *IEEE Trans. Ind. Inform.* **2018**, *14*, 1469–1481. [CrossRef]
2. Liu, T.; Yu, H.; Guo, H.; Qin, Y.; Zou, Y. Online Energy Management for Multimode Plug-In Hybrid Electric Vehicles. *IEEE Trans. Ind. Inform.* **2019**, *15*, 4352–4361. [CrossRef]
3. Chan, C.C. The State of the Art of Electric, Hybrid, and Fuel Cell Vehicles. *Proc. IEEE* **2007**, *95*, 704–718. [CrossRef]
4. Kendall, K.; Kendall, M.; Liang, B.; Liu, Z. Hydrogen vehicles in China: Replacing the Western Model. *Int. J. Hydrogen Energy* **2017**, *42*, 30179–30185. [CrossRef]
5. Mendis, N.; Muttaqi, K.M.; Perera, S.; Kamalasadan, S. An Effective Power Management Strategy for a Wind–Diesel–Hydrogen-Based Remote Area Power Supply System to Meet Fluctuating Demands Under Generation Uncertainty. *IEEE Trans. Ind. Appl.* **2015**, *51*, 1228–1238. [CrossRef]
6. Jooshaki, M.; Abbaspour, A.; Fotuhi-Firuzabad, M.; Moeini-Aghtaie, M.; Lehtonen, M. MILP Model of Electricity Distribution System Expansion Planning Considering Incentive Reliability Regulations. *IEEE Trans. Power Syst.* **2019**, *34*, 4300–4316. [CrossRef]
7. Robledo, C.B.; Oldenbroek, V.; Abbruzzese, F.; van Wijk, A.J.M. Integrating a hydrogen fuel cell electric vehicle with vehicle-to-grid technology, photovoltaic power and a residential building. *Appl. Energy* **2018**, *215*, 615–629. [CrossRef]
8. El-Taweel, N.A.; Khani, H.; Farag, H.E.Z. Hydrogen Storage Optimal Scheduling for Fuel Supply and Capacity-Based Demand Response Program Under Dynamic Hydrogen Pricing. *IEEE Trans. Smart Grid* **2019**, *10*, 4531–4542. [CrossRef]
9. Khani, H.; El-Taweel, N.A.; Farag, H.E.Z. Supervisory Scheduling of Storage-Based Hydrogen Fueling Stations for Transportation Sector and Distributed Operating Reserve in Electricity Markets. *IEEE Trans. Ind. Inform.* **2020**, *16*, 1529–1538. [CrossRef]
10. Liu, Z.; Wen, F.; Ledwich, G. Optimal Planning of Electric-Vehicle Charging Stations in Distribution Systems. *IEEE Trans. Power Deliv.* **2013**, *28*, 102–110. [CrossRef]
11. Luo, C.; Huang, Y.-F.; Gupta, V. Stochastic Dynamic Pricing for EV Charging Stations With Renewable Integration and Energy Storage. *IEEE Trans. Smart Grid* **2018**, *9*, 1494–1505. [CrossRef]
12. Xiao, Y.; Wang, X.; Pinson, P.; Wang, X. A Local Energy Market for Electricity and Hydrogen. *IEEE Trans. Power Syst.* **2018**, *33*, 3898–3908. [CrossRef]
13. Yuan, W.; Huang, J.; Zhang, Y.J. Competitive Charging Station Pricing for Plug-In Electric Vehicles. *IEEE Trans. Smart Grid* **2015**, *8*, 627–639. [CrossRef]
14. Ghosh, A.; Aggarwal, V. Control of Charging of Electric Vehicles Through Menu-Based Pricing. *IEEE Trans. Smart Grid* **2018**, *9*, 5918–5929. [CrossRef]
15. Chau, C.-K.; Elbassioni, K.; Tseng, C.-M. Drive Mode Optimization and Path Planning for Plug-In Hybrid Electric Vehicles. *IEEE Trans. Intell. Transp. Syst.* **2017**, *18*, 3421–3432. [CrossRef]
16. Dong, X.; Mu, Y.; Jia, H.; Wu, J.; Yu, X. Planning of Fast EV Charging Stations on a Round Freeway. *IEEE Trans. Sustain. Energy* **2016**, *7*, 1452–1461. [CrossRef]
17. Chen, T.; Zhang, B.; Pourbabak, H.; Kavousi-Fard, A.; Su, W. Optimal Routing and Charging of an Electric Vehicle Fleet for High-Efficiency Dynamic Transit Systems. *IEEE Trans. Smart Grid* **2018**, *9*, 3563–3572. [CrossRef]
18. Morlock, F.; Rolle, B.; Bauer, M.; Sawodny, O. Time Optimal Routing of Electric Vehicles Under Consideration of Available Charging Infrastructure and a Detailed Consumption Model. *IEEE Trans. Intell. Transp. Syst.* **2020**, *21*, 5123–5135. [CrossRef]
19. Ammous, M.; Belakaria, S.; Sorour, S.; Abdel-Rahim, A. Joint Delay and Cost Optimization of In-Route Charging for On-Demand Electric Vehicles. *IEEE Trans. Intell. Veh.* **2020**, *5*, 149–164. [CrossRef]
20. Khuller, S.; Malekian, A.; Mestre, J. To fill or not to fill: The gas station problem. *ACM Trans. Alg.* **2011**, *7*, 36. [CrossRef]
21. Pourazarm, S.; Cassandras, C.G. Optimal Routing of Energy-Aware Vehicles in Transportation Networks With Inhomogeneous Charging Nodes. *IEEE Trans. Intell. Transp. Syst.* **2018**, *19*, 2515–2527. [CrossRef]
22. Zhang, H.; Qi, W.; Hu, Z.; Song, Y. Planning hydrogen refueling stations with coordinated on-site electrolytic production. In Proceedings of the 2017 IEEE Power & Energy Society General Meeting (PESGM), Chicago, IL, USA, 16–20 July 2017; pp. 1–5.
23. Tao, Y.; Qiu, J.; Lai, S.; Zhang, X.; Wang, G. Collaborative Planning for Electricity Distribution Network and Transportation System Considering Hydrogen Fuel Cell Vehicles. *IEEE Trans. Transp. Electrif.* **2020**, *6*, 1211–1225. [CrossRef]
24. Zhao, T.; Li, Y.; Pan, X.; Wang, P.; Zhang, J. Real-Time Optimal Energy and Reserve Management of Electric Vehicle Fast Charging Station: Hierarchical Game Approach. *IEEE Trans. Smart Grid* **2018**, *9*, 5357–5370. [CrossRef]

25. Long, T.; Jia, Q.-S. Joint Optimization for Coordinated Charging Control of Commercial Electric Vehicles Under Distributed Hydrogen Energy Supply. *IEEE Trans. Control Syst. Technol.* **2022**, *30*, 835–843. [CrossRef]
26. Yang, Q.; Sun, S.; Deng, S.; Zhao, Q.; Zhou, M. Optimal Sizing of PEV Fast Charging Stations With Markovian Demand Characterization. *IEEE Trans. Smart Grid* **2019**, *10*, 4457–4466. [CrossRef]
27. de Quevedo, P.M.; Munoz-Delgado, G.; Contreras, J. Impact of Electric Vehicles on the Expansion Planning of Distribution Systems Considering Renewable Energy, Storage, and Charging Stations. *IEEE Trans. Smart Grid* **2019**, *10*, 794–804. [CrossRef]
28. Yao, W.; Chung, C.Y.; Wen, F.; Qin, M.; Xue, Y. Scenario-Based Comprehensive Expansion Planning for Distribution Systems Considering Integration of Plug-in Electric Vehicles. *IEEE Trans. Power Syst.* **2016**, *31*, 317–328. [CrossRef]
29. Li, Z.; Guo, Q.; Sun, H.; Wang, J. Coordinated Economic Dispatch of Coupled Transmission and Distribution Systems Using Heterogeneous Decomposition. *IEEE Trans. Power Syst.* **2016**, *31*, 4817–4830. [CrossRef]
30. Guerrero, J.M.; Chandorkar, M.; Lee, T.-L.; Loh, P.C. Advanced Control Architectures for Intelligent Microgrids—Part I: Decentralized and Hierarchical Control. *IEEE Trans. Ind. Electron.* **2013**, *60*, 1254–1262. [CrossRef]
31. Cheng, C.; Peng, C.; Zhang, T. Fuzzy K-Means Cluster Based Generalized Predictive Control of Ultra Supercritical Power Plant. *IEEE Trans. Ind. Inform.* **2021**, *17*, 4575–4583. [CrossRef]
32. Huang, W.; Du, E.; Capuder, T.; Zhang, X.; Zhang, N.; Strbac, G.; Kang, C. Reliability and Vulnerability Assessment of Multi-Energy Systems: An Energy Hub Based Method. *IEEE Trans. Power Syst.* **2021**, *36*, 3948–3959. [CrossRef]
33. Wu, Q.H.; Qin, Y.J.; Wu, L.L.; Zheng, J.H.; Li, M.S.; Jing, Z.X.; Zhou, X.X.; Wei, F. Optimal operation of integrated energy systems subject to the coupled demand constraints of electricity and natural gas. *CSEE J. Power Energy Syst.* **2019**, *6*, 444–457. [CrossRef]
34. Wang, W.; Huang, S.; Zhang, G.; Liu, J.; Chen, Z. Optimal Operation of an Integrated Electricity-heat Energy System Considering Flexible Resources Dispatch for Renewable Integration. *J. Mod. Power Syst. Clean Energy* **2021**, *9*, 699–710. [CrossRef]
35. Yang, W.; Liu, W.; Chung, C.Y.; Wen, F. Coordinated Planning Strategy for Integrated Energy Systems in a District Energy Sector. *IEEE Trans. Sustain. Energy* **2020**, *11*, 1807–1819. [CrossRef]
36. Chen, J.; Zhang, W.; Li, J.; Zhang, W.; Liu, Y.; Zhao, B.; Zhang, Y. Optimal Sizing for Grid-Tied Microgrids With Consideration of Joint Optimization of Planning and Operation. *IEEE Trans. Sustain. Energy* **2018**, *9*, 237–248. [CrossRef]